Journal of Nuclear Materials 512 (2018) 246–251

Contents lists available at ScienceDirect

Journal of Nuclear Materials

journal homepage: www.elsevier.com/locate/jnucmat

Effects of interstitial defects on stress-driven grain boundary migration in bcc tungsten

Liang-Liang Niu [a], Qing Peng [b], Fei Gao [b], Zhe Chen [c], Ying Zhang [d, *], Guang-Hong Lu [d]

[a] Institute of Chemical Materials, Chinese Academy of Engineering Physics, Mianyang, 621999, China
[b] Department of Nuclear Engineering and Radiological Science, University of Michigan, Ann Arbor, MI, 48109, USA
[c] Southwestern Institute of Physics, P.O. Box 432, Chengdu, 610041, China
[d] Department of Physics, Beihang University, Beijing, 100191, China

HIGHLIGHTS

- Self-interstitials can facilitate or retard stress-driven grain boundary migration.
- Helium interstitials retard stress-driven grain boundary migration.
- A transition from coupled migration to pure sliding at high helium concentrations is revealed.

ARTICLE INFO

Article history:
Received 5 July 2018
Received in revised form
25 September 2018
Accepted 9 October 2018
Available online 10 October 2018

ABSTRACT

We demonstrate via atomistic simulations that the addition of interstitial defects, either self-interstitials or helium can induce jog formation at grain boundary dislocations in bcc tungsten. For the two typical GBs with distinct dislocation structures, we show that the critical stress for stress-driven grain boundary migration is governed by the competition between the impeding effect of vacancy/helium and the facilitating effect of jogs depending on the grain boundary character, thus yielding different response of critical stress to defect concentrations. Specifically, for self-interstitials, the impeding effect of nucleated vacancies dominates in the $\sum$85 GB, while the facilitating effect of jogs dominates in the $\sum$13 GB; for helium, the impeding effect of helium plays a dominant role in both GBs. Moreover, we reveal a transition from coupled migration to pure sliding at high helium concentrations.

1. Introduction

Grain boundaries (GBs) are ubiquitous in polycrystalline materials. Stress-driven grain boundary migration (GBM) has now been well-accepted as an important mechanism operating in many physical processes such as plastic deformation, grain growth, recrystallization and phase transformations [1–5]. Notably, this mechanism, in many cases, manifests itself as the coupling between GB in-plane translation and GB normal migration, defined by a coupling factor depending solely on GB geometry [6]. Using atomistic simulations, the effects of misorientation [6,7], inclination [8,9], symmetry [10,11], temperature [6,12–16], strain rate [12,13,15], system size [6,12,13,17] and structural phase [16,18] on GBM have been extensively studied.

Tungsten (W) is the leading candidate for plasma-facing materials in future nuclear fusion reactors. A large amount of defects will be produced in W due to the irradiation of energetic neutrons and hydrogen/helium plasma [19–23]. It is known that GBs are effective sinks for point defects [24–30] and they have significant impacts on defect evolution [31,32]. A previous study proposed that GBM under mechanical or thermal stress might serve as a self-healing mechanism for W under irradiation [33]. However, the influence of point defects on GBM in W has received little attention. Thus, it is unclear whether the proposed self-healing mechanism is feasible given the complex defect environment.

Previously, Elsener et al. [34] investigated the effect of oxygen on coupled GBM and established a positive linear correlation between critical shear stress and the number of oxygen atoms. Borovikov and coworkers [35] showed that self-interstitial atoms (SIAs) and vacancies can influence the GB mobility. However, the underlying atomistic mechanisms of this influence have not been revealed. Besides, it is unclear as to how impurities such as helium

* Corresponding author.
E-mail address: zhyi@buaa.edu.cn (Y. Zhang).

https://doi.org/10.1016/j.jnucmat.2018.10.014
0022-3115/

(He) affect the GB mobility. Therefore, atomistic simulations in conjunction with an embedded-atom method potential for W have been used to investigate the influence of self-interstitial atoms and He interstitial defects on the critical stress and the underlying atomistic mechanism of GBM. We demonstrate that the critical stress for GBM is primarily controlled by the competition between the impeding effect of vacancy/He and the facilitating effect of jogs. Because of this complexity, the critical stress as a function of defect concentration do not follow a linear correlation. A transition from coupled GBM to pure GB sliding at larger He concentrations has also been revealed.

2. Methodology

The LAMMPS [36] and OVITO packages are respectively adopted for simulation and visualization. The equilibrium $\sum 85[100](07\bar{6})$ and $\sum 13[100](01\bar{5})$ symmetric tilt GBs, with effective misorientation angles of 8.8° and 22.6° and system sizes of $8\,L_{[100]} \times 8\,L_{[07\text{-}6]} \times 2\,L_{[067]}$ (20664 atoms) and $10\,L_{[100]} \times 12\,L_{[01\text{-}5]} \times 2\,L_{[051]}$ (12480 atoms) are presented in Fig. 1a and b, respectively. The most notable difference between the two GBs is the dislocation contents: ½<111>{110} for the ∑85 and <100> for the ∑13 GB. The interatomic potential for W-W interaction [37,38] produces defect properties in good agreement with experimental and *ab initio* values [39]. Periodic boundary conditions are applied parallel to the GB interface. The top and bottom slabs of ~12 Å thick (over twice the cutoff radius) are frozen (Fig. 1c). Constant velocities of 0.1 m/s for ∑85 GB and 0.2 m/s for ∑13 GB are subsequently applied to the upper slab along $+z$ direction with the lower slab remaining fixed. The metric of per-atom potential energy is used to track the GB displacement. The standard viral stress tensor expression implemented in LAMMPS is employed to calculate the shear stress. To suppress the thermal noises, all simulations are conducted at a low temperature of 0.1 K with a timestep of 2 fs. Self- and helium-interstitials are randomly created within 5 Å of the GB plane, followed by a dynamic relaxation at 300 K for 100 ps before cooling down. Note that the critical stress for GBM is defined as the peak shear stress at the shear stress-time relations.

3. Results and discussion

3.1. Effects of self-interstitial atoms

The shear stress and GB displacement as a function of time at different SIA concentrations, as well as the dependence of the critical stress on the SIA concentration are illustrated in Fig. 2. For the ∑85 GB, when 10 SIAs are loaded, the critical stress of GBM is slightly decreased. whereas the critical stress is significantly increased when 60 SIAs are loaded. It can be seen from Fig. 2c that in most scenarios, the critical stress of GBM with SIAs is increased in comparison to that of the pure GB. In contrast, we observed a universal decrease of critical stress for the ∑13 GB (Fig. 2f), indicating a facilitating effect of SIAs on GBM. In both GBs, the critical stress is not a simple monotonic correlation with SIA concentration, suggesting that multiple factors might be in play. To find out the origin of this discrepancy, we visualized the GBM process of typical simulations. As shown in Fig. 3a and b, the migration of pure ∑85 and ∑13 GBs is in fact the gliding of an array of straight dislocations (see also Supplementary Movies 1 and 2), the nature of SIAs are dislocation-based, and jogs are formed in the dislocations due to the addition of SIAs (see also Supplementary Movies 3 and 4). Previous atomistic studies by Kolluri and Demkowicz [40] also demonstrated that the migration of vacancies and self-interstitials in Cu-Nb interface are dislocation-based.

Notably, the jogs are formed for all the cases we introduced the SIAs. When there are only jog formation, the critical stress are always smaller than that of the pure GB, for example, when 10 and 30 SIAs are introduced into the ∑85 GB (Fig. 2c). In other words, the jogs act as the facilitators of GB motion. At certain concentrations, vacancies are nucleated besides jog formation, in which situation the critical stress can drop or increase depending on how many jogs are formed and how many vacancies are nucleated. For example, when 190 and 200 SIAs are introduced into the ∑85 GB. There are only one vacancy nucleation for the 190-SIA case (Fig. 3c), in which the critical stress is smaller than that of the pure GB (Fig. 2c); while six vacancies are nucleated for the 200 SIA case (Fig. 3d), in which the critical stress is higher than that of the pure GB (Fig. 2c). When vacancies are nucleated, the vacancies do not follow the GB migration and act as inhibitors. As we can see from Fig. 2c and f, for the ∑85 GB, the impeding effect of vacancies dominate for most cases. The occasional decrease of the critical stress is due to the facilitating effect of jogs when few vacancies are nucleated. We observed similar phenomena in the ∑13 GB. A typical example is illustrated in Fig. 3e, in which three vacancies are nucleated from the 70-SIA loaded accompanied by a relatively high critical stress (see also Supplementary Movies 5 and 6 for other examples). The observed universal decrease of the critical stress for all cases (Fig. 2f) is due to the much stronger jog-facilitating effect than the impeding effect of vacancies.

Supplementary video related to this article can be found at https://doi.org/10.1016/j.jnucmat.2018.10.014.

Therefore, the competition between the jog-facilitating effect and the vacancy-impeding effect determines the critical stress for the stress-driven GBM process upon SIA loading. It is worth noting that, despite the promotion or inhibition of GBM, we have not found a fundamental change of the migration mode and the corresponding coupling factor, which is characterized by the slope of the displacement-time correlation. Borovikov et al. [35] reported that the introduction of SIAs can sometimes induce a reverse of GB coupled motion indicating a transition of coupling mode, and pure GB sliding was also observed. Here we have not observed such phenomena. The possible cause of this discrepancy might be the difference in simulation conditions such as temperature. Borovikov et al. [35] employed a temperature of 1000 K which is much more relevant to fusion condition, while the present work adopted a temperature of 0.1 K to suppress thermal noises with a focus on the atomistic mechanism.

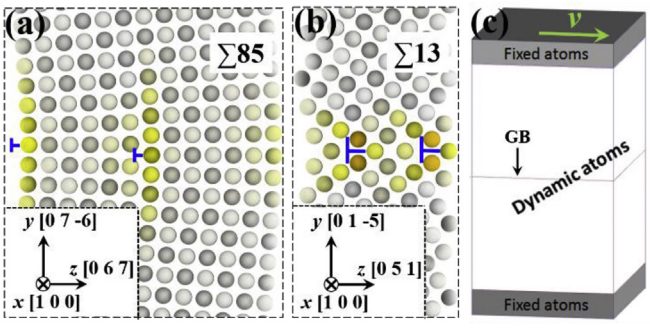

Fig. 1. (a) Equilibrium $\sum 85[100](07\bar{6})$ GB projected onto the (100) plane. The perfect GB dislocations are mixed $1/2\langle 111\rangle\{110\}$, and only the pure edge part is shown. (b) Equilibrium $\sum 13[100](01\bar{5})$ GB projected onto the (100) plane. The perfect GB dislocations are of pure edge type $\langle 100\rangle\{100\}$. For both GBs, only one periodicity along z axis is illustrated and brighter colors indicate higher potential energies. (c) Schematic of the stress-driven GBM process. (For interpretation of the references to color in this figure legend, the reader is referred to the Web version of this article.)

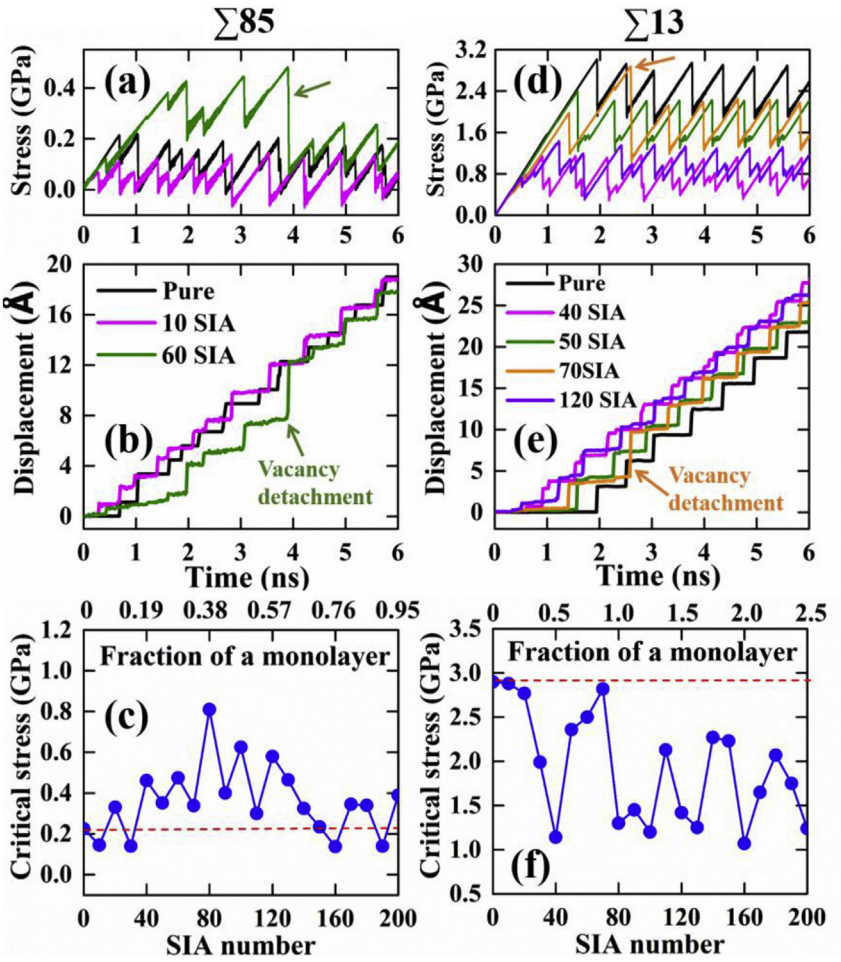

Fig. 2. (a) Shear stress and (b) GB displacement as a function of time for the ∑85 GB. (c) Critical stress as a function of SIA number for the ∑85 GB. The same descriptions apply to the case of ∑13 GB presented as (d)–(f). The red dashed lines denote the critical stress levels without SIA defects. The arrows indicate the moments when the GBs break away from the vacancies. (For interpretation of the references to color in this figure legend, the reader is referred to the Web version of this article.)

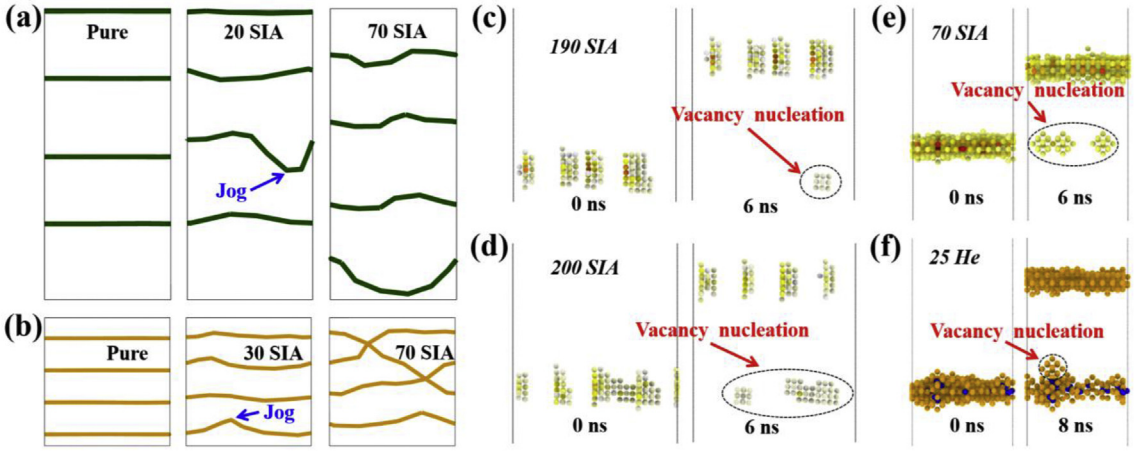

Fig. 3. Formation of jogs after SIA absorption by the (a) ∑85 and (b) ∑13 GBs. Dislocations are projected onto the GB normal direction. The same scales are used for both GBs. (c) Nucleation of a single vacancy at the stress-driven migration of the ∑85 GB after the introduction of 190 SIAs (projected onto *z* direction). (d) Nucleation of six vacancies at the stress-driven migration of the ∑85 GB after the introduction of 200 SIAs (projected onto *z* direction). (e) Nucleation of three vacancies at the stress-driven migration of the ∑13 GB after the introduction of 70 SIAs (projected onto *z* direction). (f) Nucleation of one vacancy at the stress-driven migration of the ∑13 GB after the introduction of 25 He atoms (projected onto *x* direction). The He atoms are colored deep blue. A single vacancy is denoted by the 14-atom cluster. (For interpretation of the references to color in this figure legend, the reader is referred to the Web version of this article.)

3.2. Effects of interstitial helium

We further investigate the dependence of critical stress on the He concentrations. The shear stress and GB displacement as a function of time are shown in Fig. 4 at different He concentrations, and the dependence of critical stress on the He concentration has also been presented. Regarding the ∑85 GB, the critical stress for GBM increases with increasing He concentration at the initial stage, but this trend stops at higher concentrations. For instance, when 70 interstitial He atoms are randomly placed into the ∑85 GB, there is a 5.5 ns stress-accumulation stage, increasing the critical stress to ~3 GPa, more than one order of magnitude higher than the pure GB case (Fig. 4a and b). Upon the release of the huge energy stored, a significant multiple jump of ~35 Å is observed (Fig. 4b), which is due to that the elastic energy stored is capable of immediately inducing many consecutive jumps. After this multiple-jump event, the GB exhibits coupled GBM as that of the pure GB (see also Supplementary Movie 7). In most our simulations, we found that He self-trapping leads to the easy production of SIAs and He-vacancy clusters at GBs, consistent with previous studies [29,41,42]. These SIAs changes the GB dislocation structure by the formation of jogs. At high He concentrations (larger than 120 He atoms), we observed the transition from coupled GBM to pure GB sliding, where there is no normal GB displacement (see also Supplementary Movie 8). Since coupling is determined by the GB dislocation structure, the transition from coupling to pure sliding indicates that He clustering severely damages the GB dislocation structure at high He concentrations.

In terms of the ∑13 GB, we observed a much smaller impeding effect and the critical stress for GBM at any He concentrations is no more than a factor of 3 (Fig. 4f) than that of the pure GB. Take the 25-He loaded one for example (Fig. 4d and e), the stress accumulation period is not that obvious and only a triple-jump event of ~7 Å can be observed (see also Supplementary Movie 9). When more than 30 He atoms are added, we easily see the transition from coupled GBM to pure GB sliding (see also Supplementary Movie 10). The concentration for this transition is much smaller than that in the ∑85 GB. Further, a single vacancy also nucleates as the GB breaks away from the He-vacancy clusters and carries the SIAs with them (Fig. 3f). As we have illustrated in Fig. 2, the formation of SIAs generally increases the critical stress for migration of the ∑85 GB, while decreases that of the ∑13 GB. We can thus understand why the overall critical stress increases upon interstitial He loading is much smaller in the ∑13 than ∑85 GB. We thus demonstrate that the competition between the impeding effect of vacancy/He and the facilitating effect of jogs (due to the generation of SIAs) dictates the GBM process when He impurities are introduced.

Supplementary video related to this article can be found at

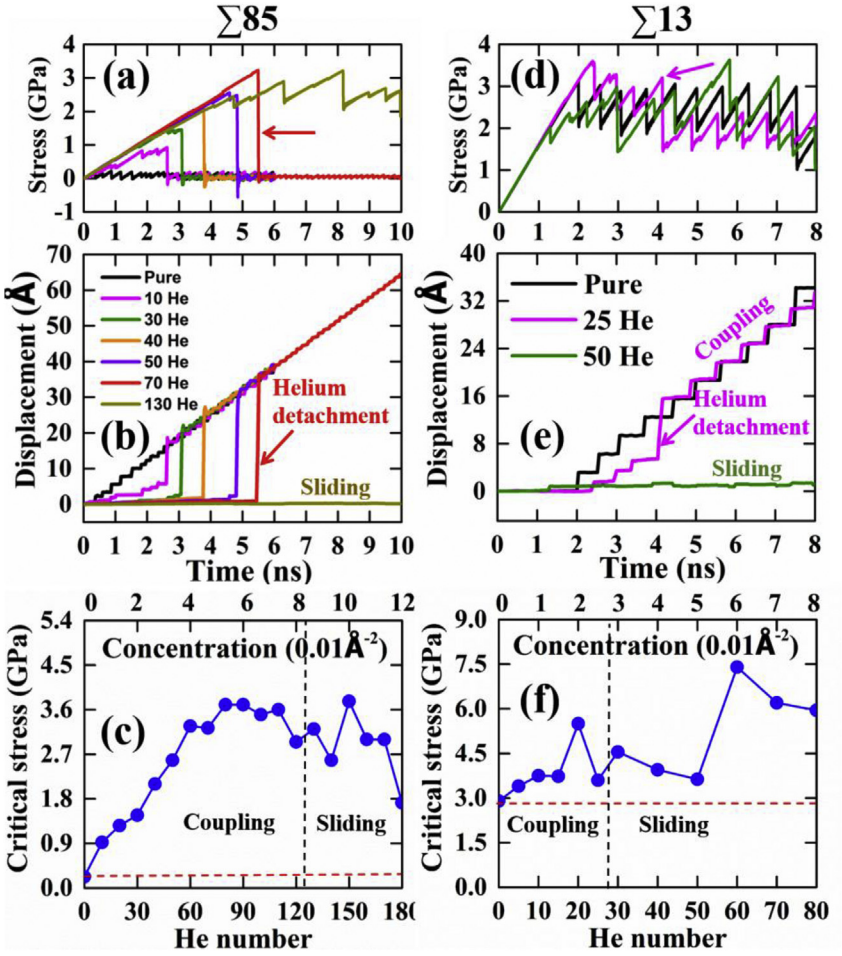

Fig. 4. (a) Shear stress and (b) GB displacement as a function of time for the ∑85 GB. (c) Critical stress as a function of He number for the ∑85 GB. The same descriptions apply to the case of ∑13 GB presented as (d)–(f). The red dashed lines denote the critical stress levels without He defects. The black dashed lines indicate the transition from coupled GBM to pure GB sliding. The arrows indicate the moments when the GBs break away from the He atoms. (For interpretation of the references to color in this figure legend, the reader is referred to the Web version of this article.)

https://doi.org/10.1016/j.jnucmat.2018.10.014.

In a recent experimental study, He et al. [43] reported that the excess of oxygen in the GBs of nanocrystalline aluminum increases the critical stress for GBM, decreases the GB mean velocity and retards grain growth, suggesting that, on the one hand, the effectiveness of stress-driven GBM as a self-healing mechanism in fusion reactor environment will likely be retarded by the low-mobility of He-vacancy clusters; but on the other hand, the retarding effect can be beneficial to the suppression of the radiation-induced grain growth of nanocrystalline W. These results provide guidance for the manipulation of the deformation mechanism and the mechanical properties of polycrystalline and nanocrystalline materials through doping.

Similar simulations have also been conducted at 300 K. The higher temperature leads to the decrease of critical stress in all cases because of the thermal effects, but the same operating mechanisms are still valid. Here we demonstrate that the correlations between critical stress and defect concentration are not linear due to the operation of the multiple effects. Because of this complexity, we show that the GB mobility can be increased or decreased depending on the GB structure and defect concentrations, in good agreement with that reported by Borovikov et al. [35] using a range of high-angle GBs. Since W is a very typical bcc metal, we expect that similar results might also be valid for other bcc metals.

4. Conclusions

We show via atomistic simulations that the nature of SIAs in a GB is dislocation-based and SIA addition leads to jog formation in bcc W. We further demonstrate that the critical stress for stress-driven GBM is governed by the competition between the impeding effect vacancy/He and the facilitating effect of jogs. Specifically, the impeding effect of vacancies dominate in the $\sum$85 GB, therefore the introduction of SIAs generally decreases the mobility of the $\sum$85 GB; while the facilitating effect of jogs plays a dominant role in the $\sum$13 GB, we thus observed an overall increase of its mobility. The introduction of He impurities increases the critical stress for the migration of both GBs, but the impeding effect is much more prominent in the $\sum$85 GB. Moreover, the addition of SIAs does not alter the coupling mode and coupling factor of GBM, while the addition of He atoms leads to the transition from coupling to pure sliding at high He concentrations due to the He clustering-induced damage of GB dislocation structure. The present results underscore the complexity of stress-driven GBM under defect influences, and contribute to the understanding of plastic deformation of polycrystalline materials, especially under harsh irradiation conditions, where a large number of defects and defect clusters are created.

Data availability statement

Data are available upon request.

Acknowledgements

This work is supported by the National Natural Science Foundation of China (NSFC) through Grant No. 51671009 and No. 11775015.

Appendix A. Supplementary data

Supplementary data to this article can be found online at https://doi.org/10.1016/j.jnucmat.2018.10.014.

References

[1] T.J. Rupert, D.S. Gianola, Y. Gan, K.J. Hemker, Experimental observations of stress-driven grain boundary migration, Science 326 (5960) (2009) 1686–1690.
[2] Y. Zhang, J.A. Sharon, G.L. Hu, K.T. Ramesh, K.J. Hemker, Stress-driven grain growth in ultrafine grained Mg thin film, Scripta Mater. 68 (6) (2013) 424–427.
[3] S.V. Bobylev, I.A. Ovid'ko, Stress-driven migration of deformation-distorted grain boundaries in nanomaterials, Acta Mater. 88 (0) (2015) 260–270.
[4] S.V. Bobylev, I.A. Ovid'ko, Stress-driven migration, convergence and splitting transformations of grain boundaries in nanomaterials, Acta Mater. 124 (2017) 333–342.
[5] S.L. Thomas, K. Chen, J. Han, P.K. Purohit, D.J. Srolovitz, Reconciling grain growth and shear-coupled grain boundary migration, Nat. Commun. 8 (1) (2017) 1764.
[6] J.W. Cahn, Y. Mishin, A. Suzuki, Coupling grain boundary motion to shear deformation, Acta Mater. 54 (19) (2006) 4953–4975.
[7] S. Tang, G. Zhang, N. Zhou, T.F. Guo, X.X. Huang, Uniaxial stress-driven grain boundary migration in Hexagonal Close-packed (HCP) metals: theory and MD simulations, Int. J. Plast. 95 (2017) 82–104.
[8] J.E. Brandenburg, L.A. Barrales-Mora, D.A. Molodov, G. Gottstein, Effect of inclination dependence of grain boundary energy on the mobility of tilt and non-tilt low-angle grain boundaries, Scripta Mater. 68 (12) (2013) 980–983.
[9] H. Zhang, D. Du, D.J. Srolovitz, Effects of boundary inclination and boundary type on shear-driven grain boundary migration, Philos. Mag. 88 (2) (2008) 243–256.
[10] L. Zhang, C. Lu, J. Zhang, K. Tieu, A dual deformation mechanism of grain boundary at different stress stages, Mater. Lett. 167 (2016) 278–283.
[11] L. Wan, S. Wang, Shear response of the Σ9<110>{221} symmetric tilt grain boundary in fcc metals studied by atomistic simulation methods, Phys. Rev. B 82 (21) (2010) 214112.
[12] Y. Mishin, A. Suzuki, B.P. Uberuaga, A.F. Voter, Stick-slip behavior of grain boundaries studied by accelerated molecular dynamics, Phys. Rev. B 75 (22) (2007) 224101.
[13] V.A. Ivanov, Y. Mishin, Dynamics of grain boundary motion coupled to shear deformation: an analytical model and its verification by molecular dynamics, Phys. Rev. B 78 (6) (2008), 064106.
[14] L.-L. Niu, X. Shu, Y. Zhang, F. Gao, S. Jin, H.-B. Zhou, G.-H. Lu, Atomistic insights into shear-coupled grain boundary migration in bcc tungsten, Mater. Sci. Eng. A 677 (2016) 20–28.
[15] J. Yin, Y. Wang, X. Yan, H. Hou, J.T. Wang, Atomistic simulation of shear-coupled motion of [1 1 0] symmetric tilt grain boundary in α-iron, Comput. Mater. Sci. 148 (2018) 141–148.
[16] L. Zhang, C. Lu, G. Michal, K. Tieu, X. Zhao, G. Deng, Influence of temperature and local structure on the shear-coupled grain boundary migration, Phys. Status Solidi 254 (4) (2017) 1600477.
[17] A. Rajabzadeh, F. Mompiou, M. Legros, N. Combe, Elementary mechanisms of shear-coupled grain boundary migration, Phys. Rev. Lett. 110 (26) (2013) 265507.
[18] T. Frolov, Effect of interfacial structural phase transitions on the coupled motion of grain boundaries: a molecular dynamics study, Appl. Phys. Lett. 104 (21) (2014) 211905.
[19] N. Castin, A. Bakaev, G. Bonny, A.E. Sand, L. Malerba, D. Terentyev, On the onset of void swelling in pure tungsten under neutron irradiation: an object kinetic Monte Carlo approach, J. Nucl. Mater. 493 (2017) 280–293.
[20] H.Y. Xu, W. Liu, G.N. Luo, Y. Yuan, Y.Z. Jia, B.Q. Fu, G. De Temmerman, Blistering on tungsten surface exposed to high flux deuterium plasma, J. Nucl. Mater. 471 (2016) 51–58.
[21] T. Koyanagi, N.A.P.K. Kumar, T. Hwang, L.M. Garrison, X. Hu, L.L. Snead, Y. Katoh, Microstructural evolution of pure tungsten neutron irradiated with a mixed energy spectrum, J. Nucl. Mater. 490 (2017) 66–74.
[22] Y. Yu-Wei, K. Xiang-Shan, W. Xuebang, C.S. Liu, J.L. Chen, G.N. Luo, Bubble growth from clustered hydrogen and helium atoms in tungsten under a fusion environment, Nucl. Fusion 57 (1) (2017), 016006.
[23] J. Zhao, X. Meng, X. Guan, Q. Wang, K. Fang, X. Xu, Y. Lu, J. Gao, Z. Liu, T. Wang, Investigation of hydrogen bubbles behavior in tungsten by high-flux hydrogen implantation, J. Nucl. Mater. 503 (2018) 198–204.
[24] X.M. Bai, A.F. Voter, R.G. Hoagland, M. Nastasi, B.P. Uberuaga, Efficient annealing of radiation damage near grain boundaries via interstitial emission, Science 327 (5973) (2010) 1631–1634.
[25] M.J. Demkowicz, R.G. Hoagland, J.P. Hirth, Interface structure and radiation damage resistance in Cu-Nb multilayer nanocomposites, Phys. Rev. Lett. 100 (13) (2008) 136102.
[26] M.A. Tschopp, M.F. Horstemeyer, F. Gao, X. Sun, M. Khaleel, Energetic driving force for preferential binding of self-interstitial atoms to Fe grain boundaries over vacancies, Scripta Mater. 64 (9) (2011) 908–911.
[27] I.J. Beyerlein, M.J. Demkowicz, A. Misra, B.P. Uberuaga, Defect-interface interactions, Prog. Mater. Sci. 74 (2015) 125–210.
[28] H. Li, Y. Qin, Y. Yang, M. Yao, X. Wang, H. Xu, S.R. Phillpot, The evolution of interaction between grain boundary and irradiation-induced point defects: symmetric tilt GB in tungsten, J. Nucl. Mater. 500 (2018) 42–49.
[29] X.-X. Wang, L.-L. Niu, S. Wang, Strong trapping and slow diffusion of helium in a tungsten grain boundary, J. Nucl. Mater. 487 (2017) 158–166.

[30] M.A. Tschopp, K.N. Solanki, F. Gao, X. Sun, M.A. Khaleel, M.F. Horstemeyer, Probing grain boundary sink strength at the nanoscale: energetics and length scales of vacancy and interstitial absorption by grain boundaries in α-Fe, Phys. Rev. B 85 (6) (2012), 064108.
[31] Z. Chen, L.-L. Niu, Z. Wang, L. Tian, L. Kecskes, K. Zhu, Q. Wei, A comparative study on the in situ helium irradiation behavior of tungsten: coarse grain vs. nanocrystalline grain, Acta Mater. 147 (2018) 100–112.
[32] G. Valles, M. Panizo-Laiz, C. González, I. Martin-Bragado, R. González-Arrabal, N. Gordillo, R. Iglesias, C.L. Guerrero, J.M. Perlado, A. Rivera, Influence of grain boundaries on the radiation-induced defects and hydrogen in nanostructured and coarse-grained tungsten, Acta Mater. 122 (2017) 277–286.
[33] V. Borovikov, X.-Z. Tang, D. Perez, X.-M. Bai, B.P. Uberuaga, A.F. Voter, Coupled motion of grain boundaries in bcc tungsten as a possible radiation-damage healing mechanism under fusion reactor conditions, Nucl. Fusion 53 (6) (2013), 063001.
[34] A. Elsener, O. Politano, P.M. Derlet, H. Van Swygenhoven, Variable-charge method applied to study coupled grain boundary migration in the presence of oxygen, Acta Mater. 57 (6) (2009) 1988–2001.
[35] V. Borovikov, X.Z. Tang, D. Perez, X.M. Bai, B.P. Uberuaga, A.F. Voter, Influence of point defects on grain boundary mobility in bcc tungsten, J. Phys. Condens. Matter 25 (3) (2013), 035402.
[36] S. Plimpton, Fast parallel algorithms for short-range molecular dynamics, J. Comput. Phys. 117 (1) (1995) 1–19.
[37] N. Juslin, B.D. Wirth, Interatomic potentials for simulation of He bubble formation in W, J. Nucl. Mater. 432 (1–3) (2013) 61–66.
[38] G.J. Ackland, R. Thetford, An improved N-body semi-empirical model for body-centred cubic transition metals, Philos. Mag. A 56 (1) (1987) 15–30.
[39] G. Bonny, D. Terentyev, A. Bakaev, P. Grigorev, D.V. Neck, Many-body central force potentials for tungsten, Model. Simulat. Mater. Sci. Eng. 22 (5) (2014), 053001.
[40] K. Kolluri, M.J. Demkowicz, Dislocation mechanism of interface point defect migration, Phys. Rev. B 82 (19) (2010) 193404.
[41] M.A. Tschopp, F. Gao, K.N. Solanki, He–V cluster nucleation and growth in α-Fe grain boundaries, Acta Mater. 124 (2017) 544–555.
[42] L. Yang, F. Gao, R.J. Kurtz, X.T. Zu, Atomistic simulations of helium clustering and grain boundary reconstruction in alpha-iron, Acta Mater. 82 (0) (2015) 275–286.
[43] M.-R. He, S.K. Samudrala, G. Kim, P.J. Felfer, A.J. Breen, J.M. Cairney, D.S. Gianola, Linking stress-driven microstructural evolution in nanocrystalline aluminium with grain boundary doping of oxygen, Nat. Commun. 7 (2016).